SAND79-0668
Unlimited Release

Compression and Extension Data for Dome Salt From West Hackberry, Louisiana

W. R. Wawersik, D. W. Hannum and H. S. Lauson
Sandia National Laboratories
Albuquerque, New Mexico 87185

Abstract

Results of six quasi-static test and four creep experiments are described in terms of standard quasi-static material properties such as uniaxial compressive strength, strain-to-failure, secant moduli, etc., and in terms of two known creep formulations. The creep formulations consist of a combined primary/secondary creep model and a purely transient creep model. All results are compared with published data for rock salt from the Jefferson Island dome and for bedded salt from the Wellington and Salado formations. They are consistent with results from these three sites suggesting that West Hackberry rock salt can be described by means of constitutive relations which are now available or currently under development. Comparative data for triaxial compression and triaxial extension also indicate that these models can be applied to predict the shear deformation of rock salt under general stress states but that modifications might be needed to predict rock salt fracture.

Table of Contents

List of Symbols and Conventions

$\sigma_1, \sigma_2, \sigma_3$	True principal stresses (force)/(current load-bearing area)--compression positive
$\varepsilon_1, \varepsilon_2, \varepsilon_3$	Engineering strains (change in length)/(original length)--contraction positive
e_1, e_2, e_3	Natural or logarithmic strains (change in length)/(current length)
$\gamma = e_1 - e_3$	Shear strain
$e = e_1 + e_2 + e_3$	Volumetric strain
e_X	Strain parallel to cylinder axis (axial strain)
$(\sigma_1 - \sigma_3)_u$	Ultimate or maximum principal stress difference
$(e_1)_u, (e_3)_u, \gamma_u, e_u$	Strains corresponding to $(\sigma_1 - \sigma_3)_u$
E_s	Secant modulus, $\frac{\Delta\sigma_1}{\Delta e_1}$ where A denotes finite stress or strain increments
E, ν, μ	Elastic constants (Young's modulus, Poisson's ratio and shear modulus)

The bulk of the data is expressed in English units consistent with SPR project requests.

List of Tables

List of Figures

Introduction

The work in this report was part of a short-term systems and engineering study to support the U. S. Strategic Petroleum Reserve (SPR) Program. Quasi-static and creep tests were conducted to aid a finite element study of the stability of an existing oil storage cavern, cavern #6 in the West Hackberry dome, West Hackberry, Louisiana. The top of the cavern is located at a depth of 3250 ft (990 m). The cavern is approximately 150 ft (46 m) high and between 334 ft (102 m) and 420 ft (128 m) in diameter. Calculations were particularly concerned with predicted creep closure of the cavern as a result of cavern depressurization from 1725 psi (11.9 MPa) to 1145 psi (7.9 MPa) at the top of the cavern wall following a fire in September, 1979. Because no site-specific data were available at the beginning of this study, all calculations were performed by means of existing material properties for rock salt from the Jefferson Island dome, Louisiana and from the bedded deposits of the Wellington formation at Lyons, Kansas.[1] The present data provide the first site-specific properties and serve to evaluate the applicability of Jefferson Island and Lyons results to West Hackberry conditions. They also permit a check of three sets of assumptions which were made in the structural calculations under this program: (1) Creep at less than approximately 90 days, including the time for dissolutioniug, is limited to transient (decelerating) creep which can be described by means of an equation of the form

$$e_1 = \alpha(\sigma_1 - \sigma_3)^m t^n$$

where e_1 and t are the greatest compressive strain and time. $(\sigma_1 - \sigma_3)$ is the principal stress difference. (2) Creep proceeds with no change in material

volume, i.e., creep data from trisxial compression tests can be used in lieu of creep data in triaxial extension which best describes the loading conditions in the walls of oil storage caverns; and (3) Temperature effects to approximately 60°C are subordinate.

Ten experiments were conducted at zero and 2000 psi (13.8 MPa) confining pressure and at 22°C temperature. Two tests at σ_3 = 2000 psi (13.8 MPa) were carried out in triaxial compression ($\sigma_2 = \sigma_3$) and two in triaxial extension ($\sigma_2 = \sigma_1$). Creep of West Hackberry salt was monitored in four tests up to 475 hours at a nominal principal stress difference of ($\sigma_1 - \sigma_3$) = 3000 psi (21 MPa).

Source of Material and Sample Description

The West Hackberry dome is located in Cameron parish in southwestern Louisiana. It is an elliptical piercement structure of Jurassic salt into eocene sediments.[2] The dome is part of a larger salt mass which is approximately 8.7 miles (14 km) long and at least 1.9 miles (3 km) wide. The top of the dome is nearly flat and located at approximately 2000 ft (625 m) below surface under up to 525 ft (164 m) of cap rock. The flanks of the dome dip from slightly less than 60° to more than 75° in the north.[2]

Core tested was taken from two drillholes, #6C and #8A into the caverns #6 and #8. Hole #6C is located 300-500 ft (100-150 m) from the northern edge of the top of the dome, Hole #8A is located more than 1000 ft (300 m) to the south of hole #6C. Both holes are identified in Figure 1 relative to the 2000 ft (625 m) contour of the dome.

Core tested was taken from depths 2200-2242 ft (671-684 m) in hole #6C and from 2300-2303 ft (701-702 m) in hole #8A. Compositions were determined on three hand specimens which appeared to be typical for the darkest least

Table I

Chemical and Dissolutioning Data[3]

%eight	Sample I.D. (Hole No.-Depth, ft.) (Sample Fraction) 6C-2208(1)	6C-2208(2)	6C-2241
% Na^+	37.7	36.5	37.5
% K^+	0.001	0.001	0.001
% Ca^+	0.272	0.360	0.271
% Mg^{++}	< 0.0001	< 0.0001	< 0.0001
% ci	58.5	57.4	58.5
% $SO_4^=$	0.65	0.86	0.66
% co;	≤ 0.005	so.005	IO.005
% HCO_3	≤ 0.005	≤ 0.005	≤ 0.005
% Insoluble Residue	1.87	3.90	2.54
Wt. of Sample (gms.)	≈ 100	≈ 100	≈ 100
Notes:	Most transparent	Darkest, visually least pure	Mix of transparent and dark salt

pure and for the most transparent clean material.[3] X-ray analyses identified only sodium chloride and anhydrite ($CaSO_4$). The results of chemical analyses are summarized in Table I. Table I suggests that all rock salt consisted of more than 93% NaCl. Considering the brine concentrations used and the stability of anhydrite,' it can also be assumed that the total anhydrite content varied between 2.7% and 5.1%. The anhydrite shown occurred primarily in steeply dipping bands in core from drillhole #6C. The width of these bands varied from 1.2 in (1.5 cm) to more than 4 in (10 cm). Core #6C also contained elongated grains with greatest dimensions between 0.24 in (6 mm) and 1.2 in (30 mm) and with aspect ratios from 1.5 to 3.5. The long axes of these grains lay approximately parallel to the anhydrite rich bands. The grain boundaries were relatively smooth indicating a moderate degree of grain interlocking. A typical sample from drillhole #6C, which was illuminated from behind, is shown in Figure 2.

Contrary to core from hole #6C, the grains in core from drillhole #8A were approximately equiaxed. They showed no preferred orientation. The grain size varied from 0.16 in to 1.2 in (4-30 mm). Specimen 8A-2302 included several large euhedral grains.

Apparatus and Experimental Procedures

Tests were performed in two identical triaxial apparatus capable of accommodating specimens up to 4 in (10.8 cm) in diameter and 8.25 in (21 cm) in length. Figure 3 is a photograph of the equipment.

Prior to testing, all specimens were covered with a 0.01-0.02 in (0.25-0.5 mm) thick layer of RTV silastic (RTV 108) for protection against the effects of humidity and to fill small surface pits or holes. This procedure is facilitated if the RTV is first thinned with toluene. After coating, each sample is placed between two steel end-caps and enclosed in an

elastomer jacket of Viton, Neoprene or EPDM. The wall thickness of these jackets is approximately 0.06 in (1.5 mm). To ensure good alignment, all specimen ends are machined flat and parallel to $\pm$ 0.001 in. ($\pm$ 0.003 mm). End effects at the interface between rock salt and end-caps are minimized by polishing the end-cap faces to a mirror finish and by coating the sample ends with thin layers of molbydenum disulfide (Molykote). All tests were started from a state of hydrostatic compression equal to the magnitude of the least principal compression σ_3 which was maintained constant.

Deviator stress was generated by increasing the axial specimens stress in triaxial compression and by increasing the radial pressure $\sigma_2 = \sigma_1$ in triaxial extension.

Axial specimen strains were monitored by means of LVDT (Linear Variable Differential Transformer) transducers parallel to the sample axes. Radial strains were measured dilatometrically and/or by means of two disc gauges. The placement of these disc gauges is demonstrated in Figure 4. Details of both techniques, calibration procedures and data reduction methods are discussed elsewhere.[5]

Quasi-static tests were performed at a mean deviatoric stress rate of $1 \leq \frac{d}{dt} (\sigma_1 - \sigma_3) \leq 2$ psi/s (7 to 14 kPa/s). This rate was approached in incremental fashion by quick, almost instantaneous changes in ram load followed by periods of several minutes during which the load was held fixed. Variations in the stress rate were caused by changes in the specimen area with changes in radial sample strains. Creep was initiated by rapid deviatoric loading in triaxial compression, $d/dt (\sigma_1 - \sigma_3) \approx 75$ psi/s (500 kPa/s). The creep stress was reached at a slightly lower rate $\frac{d}{dt} (\sigma_1 - \sigma_3) \approx 22$ psi/s (150 kPa/s) in triaxial extension.

Test Matrix

Table II shows the ten experiments described in this report. The test identification (I.D.) in the first column is used in subsequent figures and designates the following: (nominal core diameter, in) (identification of test type)/(drillhole #)-(depth, ft)/(least compressive stress, ksi)/(test temperature, °C). The abbreviated code for test type identifies four different experiments. Q: quasi-static compression test, QE: quasi-static extension test, C: triaxial compression creep test and CE: triaxial extension creep experiment. Based on elastic computations[6] the loading conditions in Table II were deemed representative for the stresses in the immediate walls of the West Hackberry cavern #6. The temperature of 60°C was suggested by well temperature measurements.[7] The values for principal stress difference and least compressive stress for four creep experiments are averages for the duration of each test.

Raw core of 4 in (10.8 cm) diameter was used for convenience in four of the quasi-static compression tests. Samples of 3.5 in. (8.9 cm) diameter were drilled for the remainder of the experiments primarily because of constraints of the available apparatus in the mode of triaxial extension.

Experimental Results

Quasi-Static Tests

The quasi-static data obtained are presented in Figures 5 through 10 using conventional graphs of principal stress difference, $(\sigma_1 - \sigma_3)$, versus greatest compressive strain, e_1, as well as cross plots of $(\sigma_1 - \sigma_3)$, y, e and time. e_1, e_3, y and e are natural strains. Denoting compressive strains positive the natural strains are obtained from measured dimensional changes and engineering strains ε_1, ε_3 as

Table II

Test Matrix

Test I.D.	Description of Test
4Q/6C-2206/0/22	Unconfined quasi-static compression, $\sigma_3 = 0$, T = 22°C
4Q/8A-2302/0/60	Unconfined quasi-static compression, $\sigma_3 = 0$, T = 60°C
4Q/8A-2301/2.0/22	Quasi-static trisxial compression, $\sigma_2 = \sigma_3 = 2000$ psi, T = 22°C
4Q/6C-2208/2.0/60	Quasi-static triaxial compression, $\sigma_2 = \sigma_3 = 2000$ psi, T = 60°C
3.5QE/6C-2241A/2.0/22	Quasi-static trisxial extension, $\sigma_2 = \sigma_1 = 2000$ psi, T = 22°C
3.5QE/6C-2223/2.0/60	Quasi-static triaxial extension, $\sigma_2 = \sigma_1 = 2000$ psi, T = 60°C
3.5C/6C-2241/2.0/22	Triaxial compression creep, $\sigma_2 = \sigma_3 = 2030$ psi, $(\sigma_1 - \sigma_3) = 2960$ Psi, T = 22°C
3.5C/6C-2201/2.0/60	Triaxial compression creep, $\sigma_2 = \sigma_3 = 2030$ psi, $(\sigma_1 - \sigma_3) = 2900$ psi, T = 60°C
3.5CE/6C-2225/2.0/22	Triaxial extension creep, $\sigma_2 = \sigma_1 \nearrow 1990$ Psi, $(\sigma_1 - \sigma_3) = 2900$ Psi, $\sigma_3 \nearrow \searrow$ T = 22°C
3.5CE/6C-2194/2.0/60	Triaxial extension creep, $\sigma_2 = \sigma_1 \nearrow 2070$ psi $(\sigma_1 - \sigma_3) = 2890$ psi, T = 60°C

Table III

Maximum Stresses and Strains of Quasi-Static Tests. Subscript u Pertains to Ultimate Stress and Strain Values.

	σ_3 (psi)	$(\sigma_1 - \sigma_3)_u$ (psi)	$(e_1)_u$ (%)	$(-e_3)_u$ (%)	$(\gamma)_u$ (%)	$(e)_u$ (%)	$(e)^*_{um}$ (%)
4Q/6C-2206/0/22	0	3790	2.5	4.0	6.5	-5.5	
4Q/8A-2302/0/60	0	3540	5.0	5.9	10.9	-6.8	-5.5
4Q/8A-2301/2.0/22	2000	> 8570	> 14.3	7 8.3	722.6	-2.3	-2.4
4Q/6C-2208/2.0/60	2000	7 7540	725.4	714.1	7 39.5	-2.8	-3.9
3.5QE/6C-2241/2.0/22	2000	76740	7 3.5	7 6.0	7 9.5	1.0	0.4
3.5QE/6C-2223/2.0/60	2000	75060	7 3.8	7 6.4	> 10.2	1.2	-0.1

* Total volumetric strain estimates based on selected measurements of final specimen dimensions.

Table IV

Summary of Deformation Characteristics of West Hackberry Dome Salt Upon First Laboratory Loading and List of Elastic Constants

Test I.D.	σ_3 (psi)	Secant Modulus (10^6 psi)/Princ. Strain Ratio $500 \leq \Delta\sigma(\text{psi}) \leq 1000$	$500 \leq \Delta\sigma(\text{psi}) \leq 2000$	Elastic (unloading) Constants $E(10^6 \text{ psi})/\nu$
4Q/6C-2206/0/22	0	0.22/-0.30	0.68/-0.68	(3.7/0.65)*
4Q/8A-2302/0/60	0	.16/-0.56	0.32/-0.71	(5.6/-)*
4Q/8A-2301/2.0/22	2000	1.75/-0.63	0.90/-0.52	$5.55^{+0.06}_{-0.22}/0.33^{+0.02}_{-0.06}$
4Q/6C-2208/2.0/60	2000	1.83/-0.30	1.05/-0.37	$5.67^{+0.25}_{-0.20}/0.31 \pm 0.3$

*Measurement made past the ultimate stress.

$$e_1 = -\ln(1 - |\varepsilon_1|)$$

$$e_3 = -\ln(1 + |\varepsilon_3|)$$

$$\gamma = e_1 - e_3$$

$$e = e_1 + e_2 + e_3$$

e and γ are volumetric and shear strains, respectively.

Figure 5 affords a comparison of the unconfined behavior of West Hackberry material at 22°C and 60°C. The steps in the two stress strain curves are results of the incremental deviatoric loading procedure described earlier. In subsequent plots stepped stress-strain curves sometimes are approximated by smooth curves which were drawn through the end points of each step, e.g., points A and B in Figure 5. It is noted that plots of principal stress difference versus shear strain and volumetric strain are the most appropriate representations to compare the results of triaxial compression and triaxial extension tests (Figures 8 through 10).

Further inspection of Figures 5 through 10 provides the supplementary data in Tables III and IV, Table III lists the unconfined strengths and the associated ultimate strains. Table III, column 3, also contains the maximum stresses below the ultimate stresses which were reached at elevated values of σ_3, It is noted that the ultimate stresses were not reached at σ_3 = 2000 psi (13.8 MPa) and greatest compression strains $e_1 \leq 25.4\%$ because the deviator stresses were still increasing when these experiments were terminated. However, observations of dilatancy* (Figure 7) imply that fracture would have developed if the experiments had been continued.

*Dilatancy denotes increases in rock volume relative to purely elastic volume changes with changes in mean stress.

In view of the ductile nature of rock salt, the non-zero volumetric strain values which were monitored in triaxial compression and triaxial extension must be considered suspect in principle. To minimize the uncertainty concerning the validity of these results, volumetric strains were calculated from two independent measurements of radial specimen deformation using dilatometric and disc gauge readings. These two sets of data are essentially identical. Additionally, the volumetric strains which were determined from records of axial and radial sample deformation were compared with volumetric strain estimates based on measurements of the final sample dimensions after testing. The latter values were entered in the last column of Table III. They constitute relatively crude estimates because of local grain bulging. With the exception of sample 6C-2223, the trend of the data in columns 7 and 8 is consistent although the quantitative agreement is poor.

Table IV contains the values of secant moduli and principal strain ratios which describe the response of West Hackberry salt upon first laboratory loading. Such values are used frequently to evaluate the behavior of rock salt from different sites. They also indicate the non-elastic nature of this material. The elastic properties of West Hackberry salt were established in rapid unloading tests at stresses below approximately 60% of the previously attained peak stress when time dependent deformation becomes subordinate.

Creep Experiments

The results of the four creep experiments are summarized in Tables V and VI and in Figures 11 and 12. Variations in the initial loading rates (column 6 of Table V) were unintentional and were primarily due to restrictions in the flow rate through hydraulic lines and in the output capacity of one of the pressure sources. In spite of these restrictions,

Table V

Summary of Data of Creep Experiments

Test I.D.	$(\sigma_1 - \sigma_3)$ (psi)	σ_3 (psi)	Initial Loading Rate (psi/s)	Test Duration (hrs)	Initial Strains (%) e_1	$-e_3$	Min. Observed Axial Creep Rate $\dot{e}_x$
3.5C/6C-2243/2.0/22	2960	2030	52.2	475	.51	0.21	9.47E-9
3.5C/6C-2201/2 0/60	2900	2030	95.7	263	.69	0.27	7.233-8
3.5CE/6C-2225/2.0/22	2900	1990	30.5	262	0.13	0.18	1.19E-8
3.5CE/6C-2196/2.0/60	2890	2070	14.5	72*	0.25	0.37	5.97E-8

*Test ran to 311 hrs; however, loading piston bottomed out after 72 hrs rendering subsequent data invalid.

Table VI

Fitting parameters for Axial Creep Strains, e_x, According to Equations (l)-(5)

Using the Correspondences $e_x \cdot |e_t|$, Cl e_o, C_2 e_a, C_3 ξ, C_4 $\dot{e}_s$ and C_1' e_o', C_2' α, C_4' n

Fit No. 1: $|e_x| = C_1 + C_2(1 - \exp(-C_3 t) + C_4 t)$; Fit No. 2: $|\dot{e}_x| = C_1' + C_2' \frac{'\sigma_1 - \sigma_3}{\mu}^{3.0} t^{C_4'}$

where $\mu = 1.8 \times 10^6$ psi (shear modulus). t denotes time in seconds.

Test I.D.	File #	Fit No.	Subscript of Constants 1	2	3	4	Standard Error of Fit
3.5C/6C-2243/2.0/22	CD8A	1	3.713-3	1.06E-2	8.623-6	1.31E-8	0.487E-3
		2	3.94E-4	3.513-3	3.00	0.528	.394E-2
3.5CE/6C-2225/2.0/22	CD9A	1	6.33E-3	9.05E-3	9.28E-6	1.13E-8	0.432E-3
		2	4.28E-3	2.06E4	3 00	0.393	.225E-3
3/5C/6C-2201/2.0/60	CD6A	1	5.96E-3	2.633-2	3 00E-5	8.93E-8	.230E-2
		2	1.05E-2	4.99E3	3.00	0.609	.173E-2
3.5CE/6C-2196/2.0/60	CD7A	1	6.55E-3	1.84E-2	5.59E-5	1.363-7	.128E-2
		2	5.04E-3	2.86E4	3.00	0.481	0.2363-3

the initial loading rates were 14 to 94 times greater than the mean loading rate in all quasi-static tests. Nevertheless, the ratios of the data in columns 2 and 6 in Table V, i.e., the stress differences divided by the initial loading strains which are equal to the secant moduli E_s, still fall into the relatively low range $4.4 \times 10^5 \leq E\ (psi) \leq 2.3 \times 10^6$ (3.0 to 16.1 GPa) and are well below the intrinsic elastic modulus $E \approx 5.6 \times 10^6$ (39 GPa) (Table IV).

Figures 11 and 12 are plots of the measured shear strains and volumetric strains versus time. The cusp in the creep curve for sample 6C-2201 (Fig. 11) is due to a gradual, 190 psi (1.3 MPa) stress drop between the 15th and 70th hour of testing when the stress was updated. This stress drop was caused by a considerable change in specimen area at constant applied force. Again, the observed volumetric strains are suspect, but no measurement errors could be identified. Increased dilatancy with an increase in temperature in the compression test in Fig. 12 is unexpected. However, this dilatancy was associated with greater shear strains than developed at 22°C. It may also be that the differences between results at ambient and elevated temperature are due to compositional and textural variations between samples. The indicated compaction in Fig. 12 for extension tests was computed independently by means of indirect and by direct measurements of radial specimen deformations. A graphical comparison of the two sets of measurements is shown in Figures 13 and 14 for samples 6C-2201 and 6C-2243. Ordinarily, the dilatometric procedure to monitor radial deformations provides the lowest volumetric strain values.

Interpretation of the creep data followed two approaches. First, all measurements of total creep strain, e_t were fitted to a combined primary/secondary creep model of the form

$$|e_t| = e_o + e_p + \dot{e}_s t \tag{1}$$

where

$$e_p = e_a(1 - e^{-\xi t}) \tag{2}$$

Here the total natural strain e_t is taken to be the axial specimen strain e_x. e_a is a saturation value, $\dot{e}_s$ is the secondary creep rate, and ξ is a relaxation frequency. Time is expressed in seconds. According to (2), e_p reaches some fraction, f of e_a when

$$t = - \frac{\ln(1 - f)}{\xi} \tag{3}$$

The choice of fit to Equations (1) and (2) is based on the analysis of a large number of results for bedded rock salt from the Salado formation in southeastern New Mexico.[8,9]

The second type of fit was often applied to the interpretation of model pillar tests and, later, to rock salt creep at constant stress:[10-14]

$$|e_t| = e_o' + \alpha t^n \tag{4}$$

where $e_t = e_x$ and

$$\alpha = \beta\left(\frac{\sigma_1 - \sigma_3}{\mu}\right)^m \tag{5}$$

The constant e_o and e_o' were used to account for initial differences in the loading rates particularly between triaxial compression and triaxial extension tests. The fitting itself was accomplished by the method of least squares.[8,15] It was also assumed that the stress exponent in Equation (5) equalled three.[10-14] The fitting parameters according to

Equations (1) through (3) are listed in Table VI. It is noted that the volumetric strains proved to be no more than 11% of the shear strains for the duration of the experiments. Therefore, setting $e \approx 0$ it follows that $e_2 = e_3 \approx -\frac{1}{2} e_1$, and $\gamma = (e_1 - e_3) \approx \frac{3}{2} e_x$. The quantity e_x is the axial sample strain. In compression $e_x = e_1$ and in extension $e_x = e_3$. The secondary creep estimates, constant $C_4 = \dot{e}_x$ in Table V, compare well with the smallest observed creep rates which were determined by means of linear least square fits to the last, approximately 50 hours of test data for each experiment (Table V). Future fits will deal directly with the experimentally monitored shear strains and volumetric strains after additional confirmations of all measurements will have been completed.

Discussion

The quasi-static data for West Hackberry salt are typical for rock salt from other sources. The salt behaves non-elastically even at low deviator stress. This is indicated by the small secant moduli $E_S \leq 2.1 \times 10^6$ psi (14.6 GPa) in Table IV compared with a Young's modulus of $E \approx 5.6 \times 10^6$ psi (39 GPa). Pressure has a strong effect on the ultimate stresses and strains over the range of confining pressures applied here, zero to 2000 psi (13.8 MPa). However, based on published data, the influence of pressure is bound to be greatest at $\sigma_3 \leq 1500$ psi (10.3 MPa) and decreases steadily as σ_3 is raised. For this reason, it was expected that the shear strains of West Hackberry samples would agree closely in triaxial compression and triaxial extension. In spite of the agreement in shear behavior, it is noted that systematic differences remained in the volumetric strain response. If these results prove to be correct as is indicated by the cross-checks of all measurements, then the observed

variations in volumetric strain response suggest persistent differences in strength between triaxial compression and extension even at relatively high σ_3. To test this point, additional experiments should be carried out to macroscopic fracture at several confining pressures up to at least 13.8 MPa.

The temperature rise from 22 to 60°C produced only a minor change in the uniaxial compressive strength (Fig. 5). In contrast, a mere 38°C change in temperature resulted in an almost twofold increase in the shear flow at elevated confining pressure (Fig. 6). The exact value of this increase is probably a function of the imposed rate of loading. However, overall it is confirmed that temperature must be considered in the choice of rock salt properties for design calculations.

Creep experiments at σ_3 = 2000 psi (13.8 MPa) produced similar results in several respects. Nearly identical behavior was monitored both at ambient temperature and at elevated temperature (Fig. 11). Nevertheless, the volumetric strain behavior (Fig. 12) was systematically different in the two types of tests. This trend in the volumetric strains suggests a preferential nucleation and alignment of microcracks which has been verified in more recent tests on rock salt from another dome. Therefore if creep rupture were to occur, then it is likely to be different in compression from what it is in extension.

The parameter listing and standard errors for the fits to the axial sample strains in Table VI demonstrate that the combined primary/secondary creep equation (1) and the purely transient creep law, Equation (4), fit the data about equally well even though the primary creep according to Equations (2) and (3) was at least 95% saturated. Considering only the present data, it follows that the unambiguous resolution of secondary creep and the choice

of the best creep law requires special tests, including long-term creep experiments. However, in the meantime, Equations (1) and (2) are favored on physical grounds and because it is likely that the omission of secondary creep leads to less conservative designs, i.e., smaller strains, particularly if the design life is long.

Because creep tests were carried out only at one stress level, it was impossible to determine the stress dependency of the creep of West Hackberry core. On the other hand, if the temperature dependence on secondary creep in Equation (1) is described by the Weertman[16] relation

$$\dot{e}_s = Ae^{-Q/RT}\left(\frac{\sigma_1 - \sigma_3}{\mu}\right)^n \qquad (6)$$

then the measurements at 22 and 60°C yield an activation energy Q = 11.4 kcal/mole (47.8 kJ/mole). R is the gas constant and T denotes absolute temperature. If the temperature dependence in Equations (4) and (5) is contained in β either as

$$\beta = \beta' T^s \qquad (7)$$

or

$$\beta = \beta'' e^{-U/RT}$$

then the average data at each test temperature implies s = 9.32 and U = 5.6 kcal/mole (23.4 kJ/mole).

It was one objective of this study to determine the comparative behavior of rock salt from West Hackberry, Jefferson Island and from the Wellington formation at Lyons. The latter comparison automatically raises the added question whether the properties of dome salt are different from those of

bedded salt because of differences in tectonic histories. Available ambient temperature data from all three sites are summarized in Table VII and in Figure 15. Several observations are readily apparent. The variation of the ultimate stresses, ultimate strains and secant moduli upon first laboratory loading in Table VII are well within the typical data scatter for large suites of tests on rock salt from any location.[17] The agreement of data is particularly good if it is considered that the results were obtained in different laboratories and on specimens of different sizes. The only apparent discrepancy appears to exist in the magnitude of the intrinsic elastic constants (column 6 in Table VII). The most likely reason is a difference in measurement techniques and experimental resolution. However, it is emphasized that the high value of Young's modulus which is reported here for West Hackberry core agrees perfectly with the Young's moduli which were computed from rock salt densities and from measured dilatational and shear wave velocities.[18] The elastic constants in Table VII also agree with those obtained for rock salt from other locations.

Figure 15 shows creep measurements to 120 hours which is the maximum test duration for core from Jefferson Island and Lyons. The creep curves for West Hackberry salt appear to be a good average for the eight curves from Jefferson Island and Lyons. Although all three sets of results differ markedly at small times, the average creep rates between 100 and 120 hours fall into the narrow range from 7.9×10^{-9} l/s for Lyons core to 2.24×10^{-8} l/s for Jefferson Island material. The average value for the ten tests shown in Figure 15 is 1.66×10^{-8} l/s. Given the fact that the creep rates between 100 and 120 hours were overlapping, it becomes obvious to suggest that the long term response of material from all three sources is essentially the same. It appears further that the true differences in creep are limited to

Table VII

Indicator Properties for Rock Salt from West Hackberry, Jefferson Island, and Lyons[13,14]

Material Source	No. of Tests or Measurements	σ_3 (psi)	$(\sigma_1 - a_3)_u$ (psi)	Secant Mod., E_s $500 \leq \Delta\sigma$ (psi) ≤ 2000 (10^6 psi)	Elastic Constants $E(10^6$ psi$)/\nu$	$(e_1)_u$ p(%)s	$\frac{d}{dt}(\sigma_1 - \sigma_3)$ i / s
West Hackberry	1	0	3780	0.67	----	2.5	1
	1	2000	7 8570	0.90	----	> 14.3	1
	6	0-2000	----	---	$5.58^{+0.33}_{-0.25}/0.32^{+0.03}_{-0.05}$	----	7 10
Jefferson Island	2	0	3120 ± 15	0.19 ± 0.01	----	2.9	0.3
	1	0	3520	0.26	----	2.9	8.3
	1	1500	7 9650	0.59	----	721.5	8.3
	2	2000	> 6900	0.39 ± 0.06	----	7 13.5	0.3
	6	0-2000	----	----	$3.03^{+0.94}_{-1.03}/0.42^{+0.09}_{-0.19}$	----	----
Lyons	3	0	3660^{+120}_{-190}	----	----	≤ 3.5	~ 2.5
	2	500	----	0.55 ± 0.1	----	----	~ 2.5
	7	500-5000	----	$7\ 0.87 \pm {}^{0.35}_{-0.44}$	----	----	~ 2.5
	2	500-2000	----	----	1.54 ± 0.07/----	----	~ 2.5

initial creep response which is probably sensitive to variations in recent sample histories in the same way that recent specimen histories are reflected in quasi-static monotonic loading experiments.[19]

The similarity between the rock salt behavior in Figure 15 is not limited to Jefferson Island, Lyons and West Hackberry data. A comparison of West Hackberry data with the best fit to tests on bedded salt from the Salado formation in New Mexico,[9] provides excellent agreement. This is shown in Figure 16 where the secondary creep estimates for West Hackberry of Table VI are plotted onto the 22 and 60°C fits to Salado salt. Somewhat fortuitously, the agreement between the four West Hackberry data points and the best Salado fits is considerably better than the agreement between these fits and several individual data points for Salado material which were ascertained in ambient temperature experiments (Fig. 16). This scatter in otherwise careful experiments helps to put the apparent divergence in measurements in Figure 15 into proper perspective.

Summary and Conclusions

Six quasi-static and four creep experiments on West Hackberry rock salt were described. All quasi-static test results, ultimate stresses and strains, elastic constants and secant moduli during first laboratory loading, were quite similar to data for rock salt from three other sources. Pressure effects are significant at low confining pressure. However, at σ_3 = 2000 psi (13.8 MPa) this effect was largely suppressed so that the shear behavior of West Hackberry salt was almost identical in triaxial compression and triaxial extension. On the other hand, systematic differences in the volumetric strains indicate that the ultimate stresses and strains might be different in the two cases

if such tests are continued to fracture. A small change in temperature from 22 to 60°C was shown to produce substantial changes in the shear flow of West Hackberry core.

Creep tests in triaxial compression and triaxial extension were analyzed in terms of combined primary/secondary creep model and in terms of a purely transient formulation which was applied in earlier West Hackberry analyses.[1] Both models described the experimental data well for the duration of the present tests ($t \leq 475$ hours). However, the combined primary/secondary interpretation was favored because it is consistent with some known flow mechanisms in halite.

Almost identical shear creep data and systematically varying volumetric creep results in compression and extension suggest that pressure does not influence the flow of salt at σ_3 = 2000 psi (13.8 MPa) but that it might alter the development of creep rupture. Temperature had a very pronounced influence much like in quasi-static tests. The comparison of creep data at 22 and 60°C implies an activation energy of Q = 11.4 kcal/mole (47.8 kJ/mole) for secondary creep and U = 5.6 kcal/mole (23.4 kJ/mole) if creep is attributed solely to transient creep. If the temperature effect in the transient creep formulation is related to a power function of temperature, T^s then s = 9.32.

Neglecting early time data, the results for West Hackberry salt compare well with creep data from the Jefferson Island dome and for bedded salt from the Wellington formation at Lyons, Kansas and from the Salado formation, southeastern New Mexico. The agreement is particularly good between secondary creep estimated for West Hackberry and Salado material suggesting that different tectonic histories had no effect.

In view of the consistency of all results, it appears that little further mechanical testing is needed on West Hackberry material unless creep fracture is deemed possible or unless particular structural, textural or compositional anomalies are encountered. Such anomalies might include cases where anhydrite is concentrated primarily within sodium chloride crystals rather than along grain boundaries. It also appears that the time dependent response of West Hackberry salt can be described by means of existing or evolving constitutive models for Salado salt.

References

1. Tillerson, J. R. and P, D. Hilton, "Long-Term Cavern Stability Evaluation," Appendix E in "Systems Integration and Engineering Support Study for the Strategic Petroleum Reserve (SPR) Program - Final Report," SPR Project Division 4701, ed., SAND79-0637, Sandia National Laboratories, 1979.

2. Federal Energy Administration (now Department of Energy), Strategic Petroleum Reserve Office, Strategic Petroleum Reserve - Final Environmental Impact Statement, West Hackberry Salt Dome, FES 76/77-4,1977.

3. Bild, R. W., unpublished data, Sandia National Laboratories, 1980.

4. Braitsch, O., Salt Deposits - Their Origin and Composition, Springer-Verlag, 1971.

5. Wawersik, W. R., "Indirect Deformation (Strain) Measurements and Calibrations in Sandia Triaxial Apparatus for Rock Testing to 250°C," SAND79-0114, Sandia National Laboratories, 1979.

6. PB/KBB, "Strategic Petroleum Reserve Program - Salt Dome Geology and Cavern Stability Analysis," Final Report to the Department of Energy, August 1978.

7. Jacobs/D'Appolonia,"Thermal Analyses, Stability Analyses and Recertification Requirements, Cavern #6, West Hackberry Site, Cameron Parish, Louisiana,' J/D-R008, Technical Direction #J/D-17, 1979.

8. Herrmann, W., W. R. Wawersik and H. S. Lauson, "Creep Curves and Fitting Parameters for Southeastern New Mexico Bedded Salt," SAND80-0087,Sandia National Laboratories, 1980.

9. Herrmann, W., W. R. Wawersik and H. S. Lauson, "Analysis of Steady State Creep of Southeastern New Mexico Bedded Salt," SAND80-0558, Sandia National Laboratories, 1980.

10. Obert, L., "Deformational Behavior of Model Pillars Made from Salt, Trona and Potash Ore," Proc. 6th U. S. Rock Mech. Symp., Univ. of Missouri, Rolla, MO, 1964.

11. Lomenick, T. F., "Laboratory Pillar Model Experiments," in "Project Salt Vault: A Demonstration of the Disposal of High Activity Solidified Wastes in Underground Salt Mines," R. L. Bradshaw and W. C. McClain, eds., ORNL-4555, Oak Ridge National Laboratory, 1971.

12. Dreyer, W., The Science of Rock Mechanics, Trans. Tech. Publications, 1972.

13. Hansen, F. D., "Quasi-static and Creep Deformation Characteristics of Bedded Salt from the Carey Mine Near Lyons,-Kansas," Tech. Memor. Report RSI-0067, RE/SPEC, Inc., Rapid City, SD, 1978.

14. Hansen, F. D., "Case History Rock Mechanics Examination of the Jefferson Island Salt Mine: II Laboratory Evaluation of Strength and Creep Deformation Characteristics of Dome Salt Under Confining Pressure," Tech. Memor. Report RSI-0057, RE/SPEC, Inc., Rapid City, SD, 1978.

15. Jefferson, T. H., "TJMAR1 - A FORTRAN Subroutine for Nonlinear Least Squares Parameter Estimation," SLA73-0305, Sandia National Laboratories, 1974.

16. Weertman, J., "Dislocation Climb Theory of Steady-State Creep," Trans. AIME, 61, 1968.

17. Dreyer, W., "Zur Druckfestigkeit von Salzgesteinen," Kali und Steinsalz, Heft 7, 243-251, 1961.

18. Wawersik, W. R., D. J. Holcomb, H. S. Lauson and D. W. Hannum, "Quasi-Static and Creep Data for Dome Salt from Bryan Mound, Texas," SAND80-1434, Sandia National Laboratories, 1980.

19. Wawersik, W. R. and D. W. Hannum, "Mechanical Behavior of New Mexico Rock Salt in Triaxial Compression to 200°C," J. Geophys. Res., 85, B2, 1980.

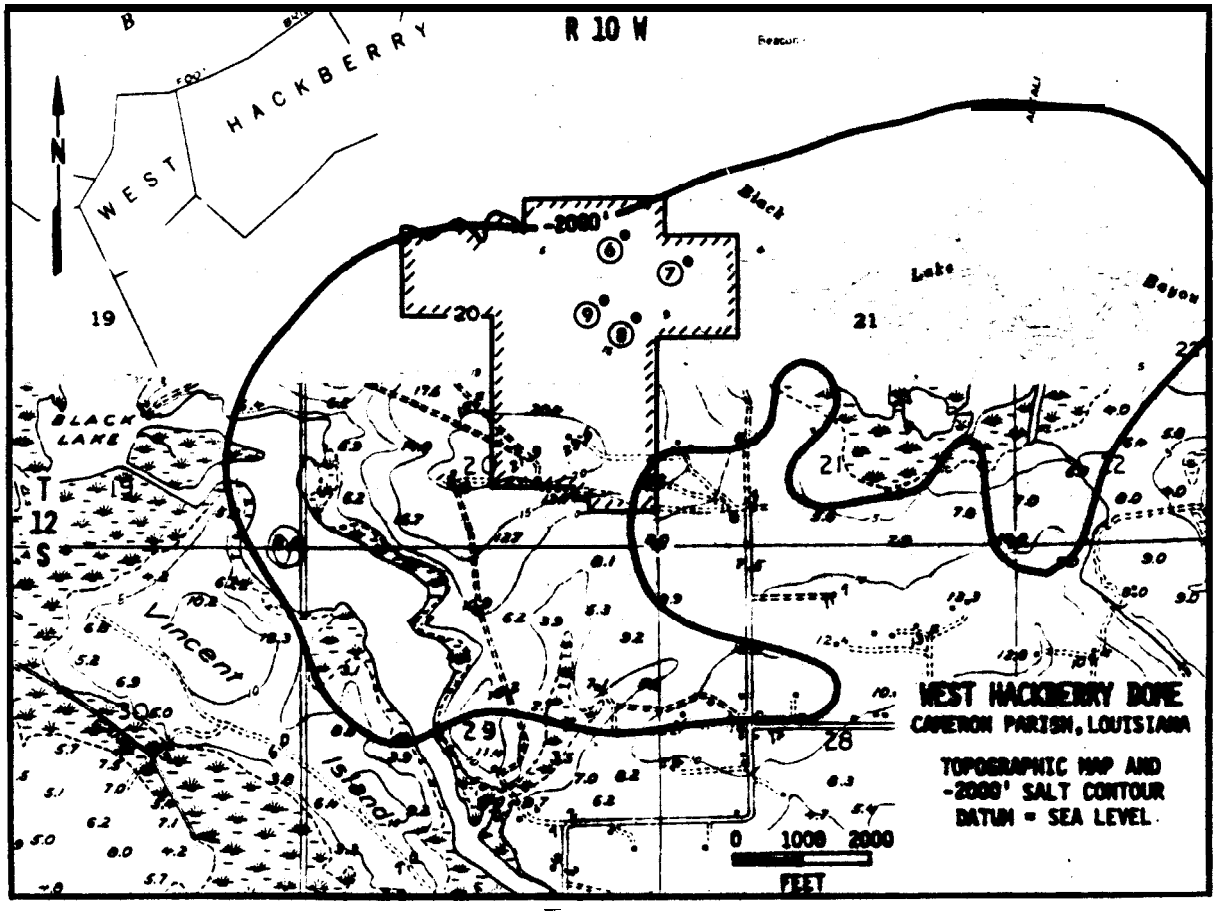

Figure 1: Map of 2000 ft (625 m) contour of West Hackberry dome. Cross hatched boundary defines DOE property line.

Figure 2: West Hackberry sample from drillhole #6C depth 2223 ft (695 m) with back illumination.

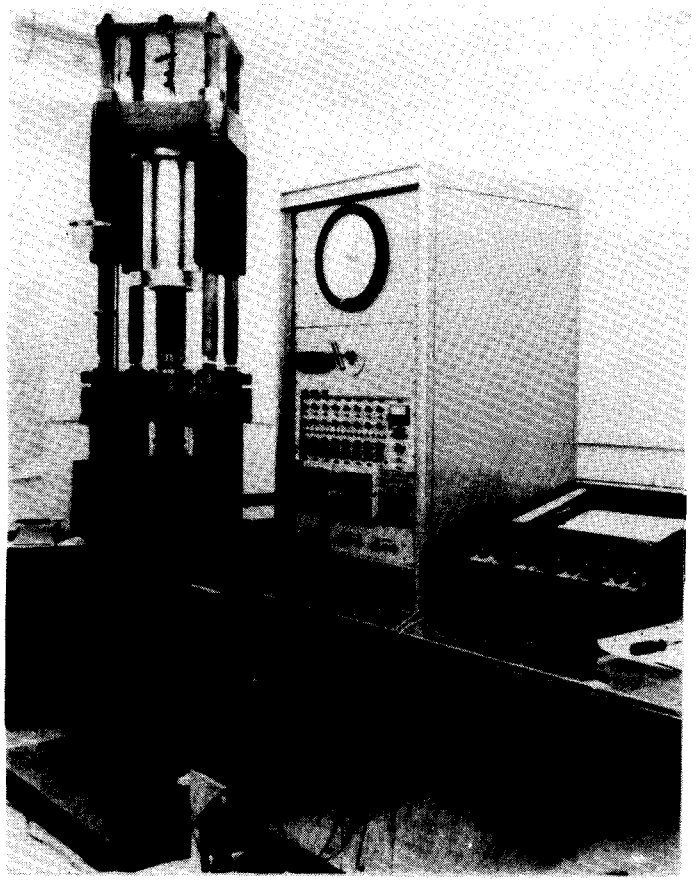

Figure 3: Triaxial test apparatus.

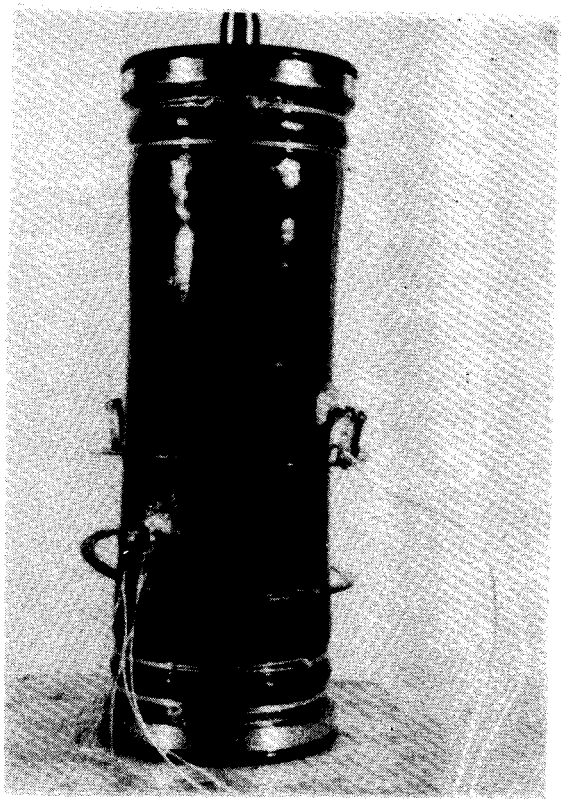

Figure 4: Extension specimen in flexible Viton jacket with two disk gauges and transfer buttons.

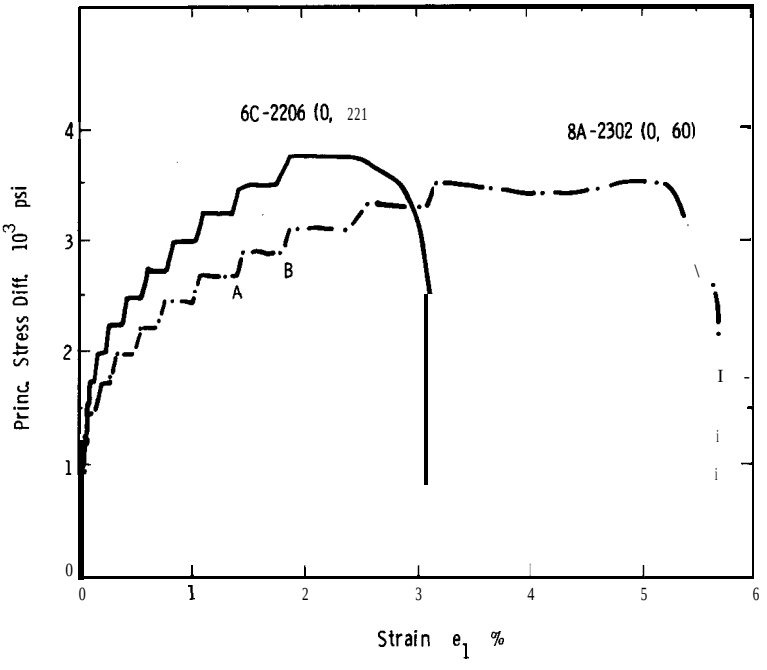

Figure 5: Principal stress difference v6. axial strain in unconfined compression tests at 22 and 60°C.

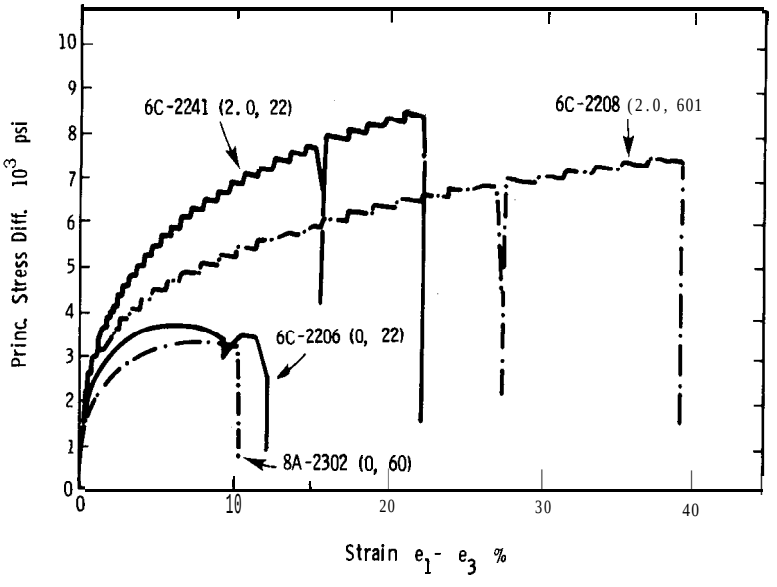

Figure 6: Principal stress difference vs. shear strain for uniaxial and triaxial compression test6 ($\sigma_2 = \sigma_3$) at 22 and 60°C.

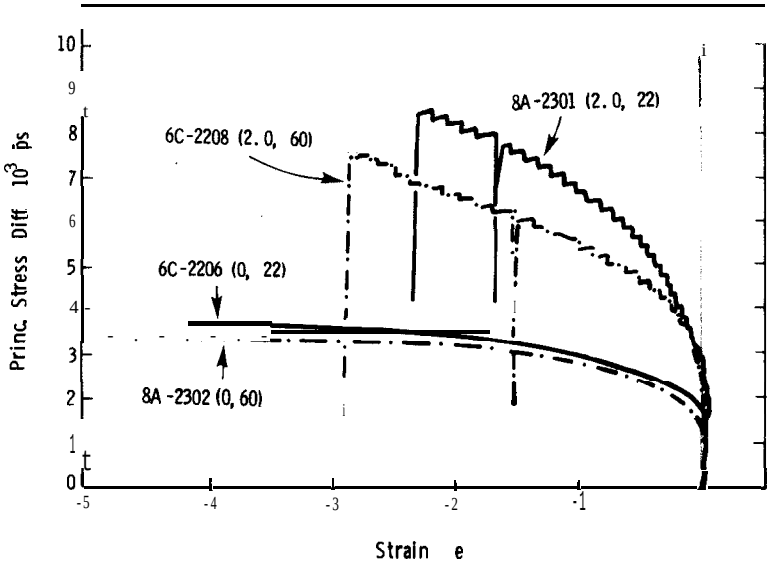

Figure 7: Principal stress difference vs. volumetric strains for uniaxial and triaxial compression tests($\sigma_2 = \sigma_3$) at 22 and 60°C.

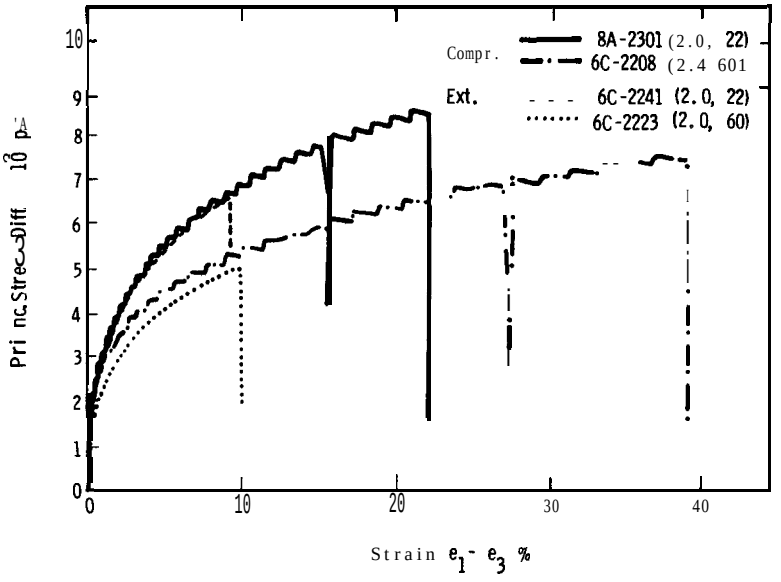

Figure 8: Comparison of triaxial compression and triaxial extension data in the space ($\sigma_1 - \sigma_3$) vs. y = ($e_1 - e_3$) at 22 and 60°C.

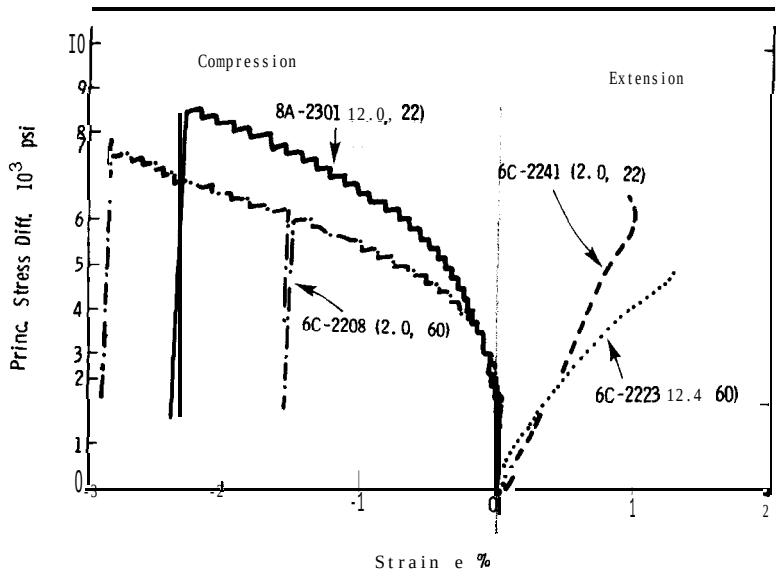

Figure 9: Comparison of triaxial compression and triaxial extension data in the space $(\sigma_1 - \sigma_3)$ vs. e at 22and 60°C.

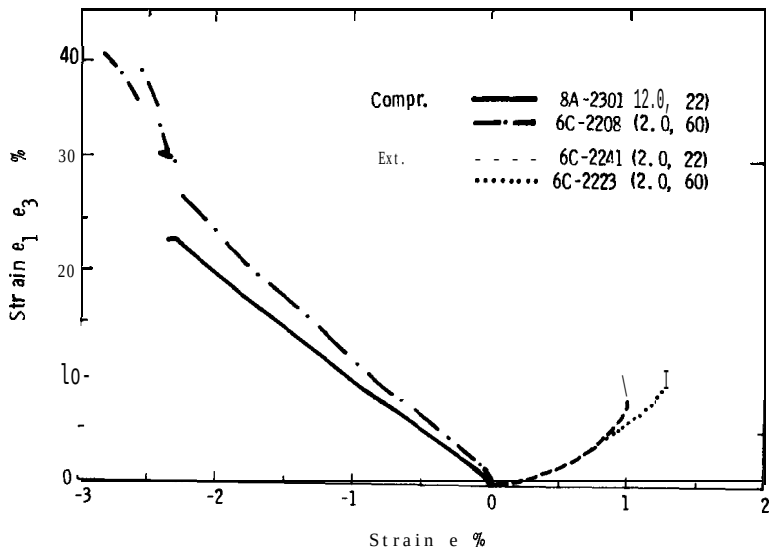

Figure 10: Comparison of biaxial compression and triaxial extension data in the space $\gamma = (e_1 - e_3)$ vs. e at 22 and 60°C.

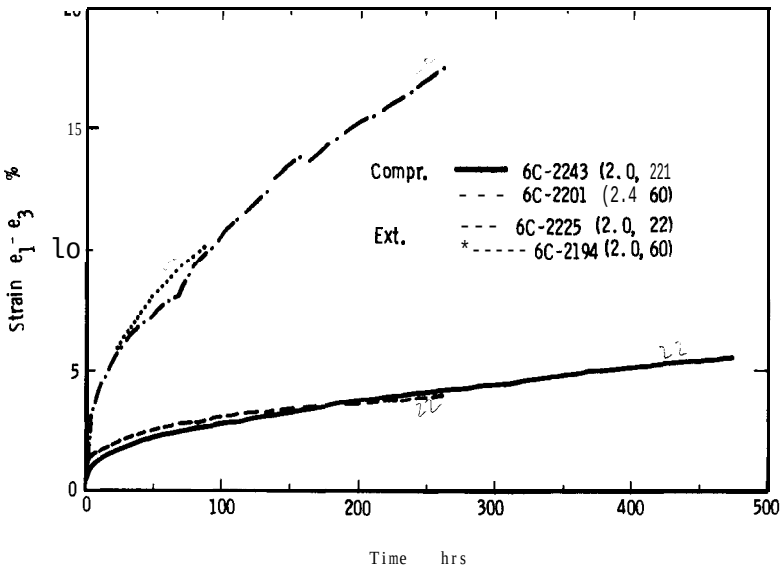

Figure 11: Shear creep in triaxial compression and triaxial extension at 22 and 60°C.

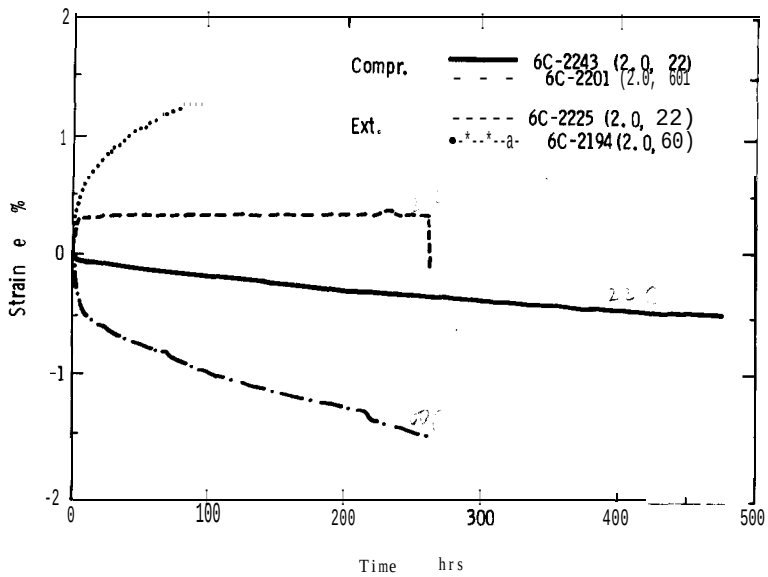

Figure 12: Volumetric creep in triaxial compression and triaxial extension at 22 and 60°C.

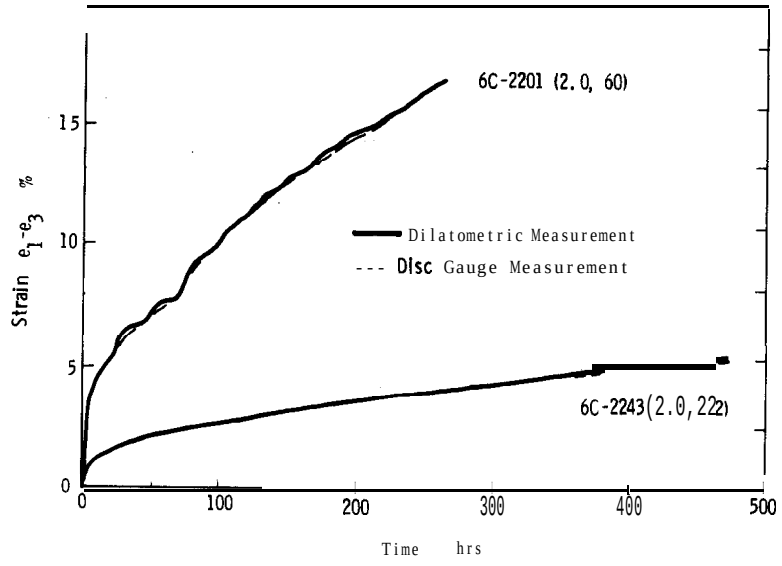

Figure 13: Comparison of shear creep based on independent measurement6 of radial sample deformations.

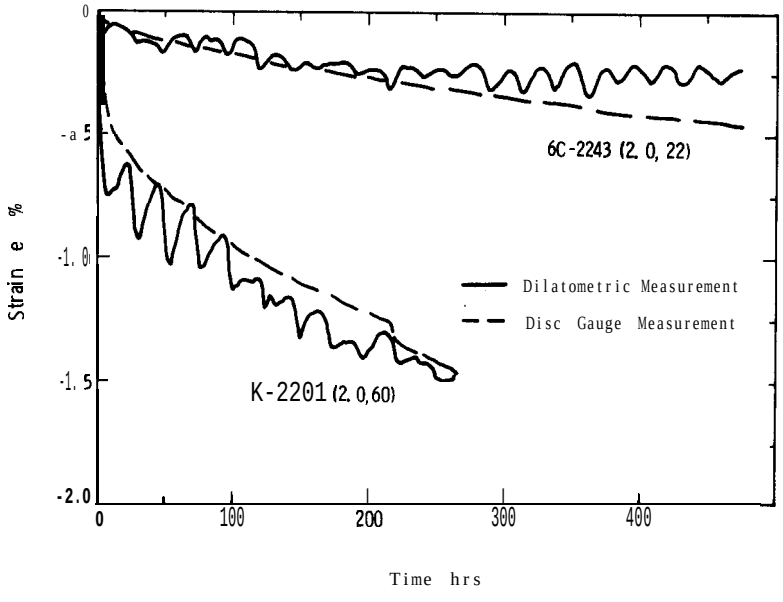

Figure 14: Comparison of volumetric creep based on independent measurements of radial sample deformations. Noise in dilatometric records is due to thermally induced volume changes of confining pressure medium.

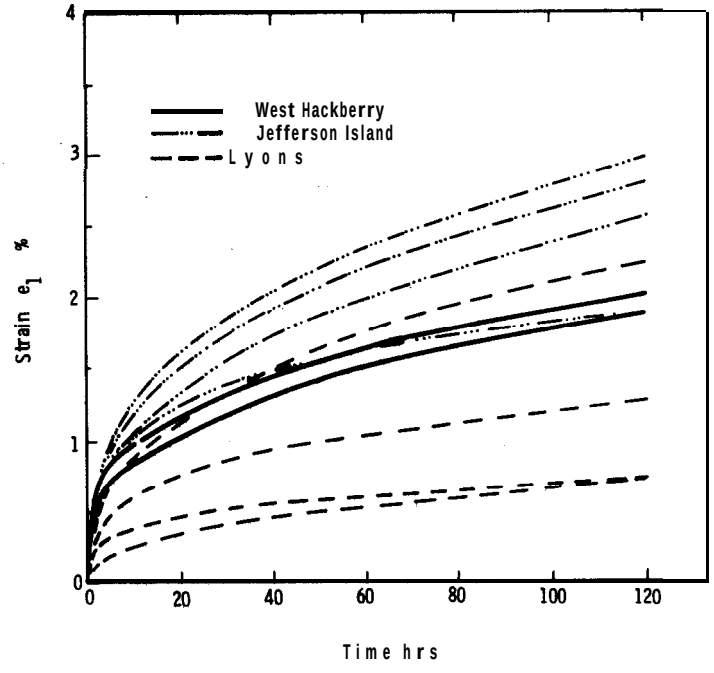

Figure 15: Comparison of axial creep data, e, vs. t for dome salt from West Hackberry and Jefferson Island, Louisiana and for bedded salt from Wellington formation, Lyons, Kansas. $(\sigma_1 - \sigma_3) = 3000$ psi, $500 \leq \sigma_3 \leq 2000$ psi.

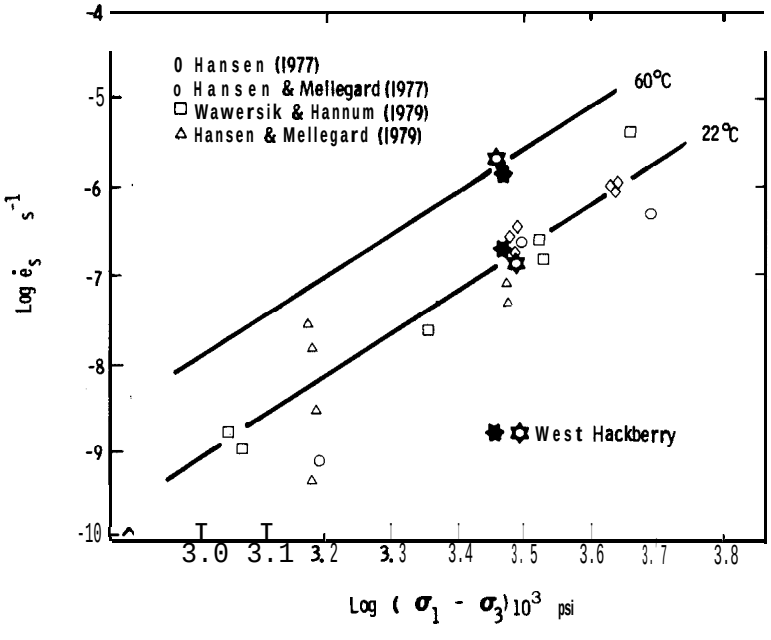

Figure 16: Comparison of secondary (steady state) creep rates for West Hackberry dome salt with bedded salt from the Salado formation, southeastern New Mexico.

Distribution: (Materials Report)
U. S. Department of Energy
Strategic Petroleum Reserve
Project Management Office
900 Commerce Road East
New Orleans, LA 70123
Attn: C. C. Johnson
R. W. Mazurkiewicz (5)
G. J. Scango
G. A. Stafford

U. S. Department of Energy
Strategic Petroleum Reserve
1726 M Street NW
Washington, DC 20461
Attn: Larry Pettis

Aerospace Corporation
800 Commerce Road East, Suite 310
New Orleans, LA 70123
Attn: Elliott Katz

Parsons-Gilbane
800 Commerce Road West
New Orleans, LA 70123
Attn: Walter Marquardt

Dravo Utility Constructors, Inc.
850 s. Clear-view Pkwy.
New Orleans, LA 70123
Attn: C. Ashline

Jacobs/D'Appolonia Engineers (2)
6226 Jefferson Hwy., Suite B
New Orleans, LA 70123
Attn: Harold Kubicek
c/o Bill Walker

Aerospace Corporation
2350 East El Segundo Blvd.
El Segundo, CA 90009
Attn: Guy F. Kuncir

R. L. Thoms
Louisiana State University
Institute for Environmental Studies
Atkinson Hall
Baton Rouge, LA 70803

4000 A. Narath
4500 E. H. Beckner
4540 M. L. Kramm
4541 L. w. Scully
4543 J. F. Ney
4543 R. R. Beasley (5)
4543 M. H. Gubbels
4745 J. R. Tillerson
5000 J. K. Galt
5500 0. E. Jones
5510 D. B. Hayes
5511 J. W. Nunziato
5520 T. B. Lane
5522 T. G. Priddy
5522 S. E. Benzley
5522 D. S. Preece
5530 W. Herrmann
5531 S. W. Key
5531 H. S. Lauson
5531 S. T. Montgomery
5531 H. S. Morgan
5532 W. R. Wawersik (15)
5532 D. W. Hannum
5820 R. E. Whan
5821 R: W: Bild
3141 T. L. Werner (5)
3151 W. L. Garner (3)
3154-3 R. P. Campbell (25)
For DOE/TIC
8266 E. A. Aas